Applied Catalysis B: Environmental 198 (2016) 124–132

Contents lists available at ScienceDirect

Applied Catalysis B: Environmental

journal homepage: www.elsevier.com/locate/apcatb

Discussion on the reaction mechanism of the photocatalytic degradation of organic contaminants from a viewpoint of semiconductor photo-induced electrocatalysis

Xin Xiao*, Shunheng Tu, Mingli Lu, Huan Zhong, Chunxia Zheng, Xiaoxi Zuo, Junmin Nan*

School of Chemistry and Environment, South China Normal University, Guangzhou Key Laboratory of Materials for Energy Conversion and Storage, Guangzhou 510006, PR China

ARTICLE INFO

Article history:
Received 28 January 2016
Received in revised form 10 May 2016
Accepted 20 May 2016
Available online 20 May 2016

Keywords:
Semiconductor photocatalysis
Photo-induced electrocatalysis
Bismuth oxyhalides
Organic contaminants
Reaction mechanism

ABSTRACT

Up to now, the well-known mechanism on the photocatalytic degradation of contaminants is mainly based on the reactions derived from the photogenerated electron-hole pairs and their subsequent oxidizing species, and the degradation of organic dyes are especially focused. Whereas, it is rarely concerned the relationship of the oxidation ability of photocatalysts with the oxidative behaviors of contaminants. In this paper, a semiconductor photo-induced electrocatalysis model is proposed to clarify the photocatalytic mechanism by correlating the band structures of BiOI, $Bi_4O_5I_2$, and $Bi_4O_5Br_2$ with their visible-light photocatalytic reactivity to phenol, bisphenol A, methylparaben, and propylparaben. It is revealed that the essential condition for degrading a certain contaminant is the valence band potential of photocatalyst is positive than the oxidation potential of contaminant. The valence band position of a photocatalyst can be determined by its optical absorption and electrochemical flat band potential measurement, and the oxidation potential of a contaminant can be measured by cyclic voltammetry technique. In particular, it is indicated that the oxidation potential of contaminants are generally correlated with their molecular orbital energy, which can be predicted by density functional theory (DFT) calculation. And the band positions of photocatalysts evaluated by an empirical equation based on the element electronegativity is in accordance with the actual band potentials. In addition, the bands composition calculated using DFT not only matches the experimental results but also provides the related information on the band structure with the chemical composition of catalysts. Thus, from the viewpoint of photo-induced electrocatalysis and with the help of experimental and theoretical analysis, the most photocatalytic reactions can be predicted and designed, which is universal for the environmental photocatalysis.

1. Introduction

In the past few decades, a large number of studies have focused on the semiconductor photocatalysis of environmental remediation [1,2]. Up to now, the mechanism for the photocatalytic degradation of organic contaminants has attracted significant attention and various hypotheses have been suggested [3–5]. It is widely accepted that the mechanism involves semiconductor absorbs photons when the photocatalyst is irradiated by sunlight or illuminated light, and if the energy of incident light is high enough, the electrons in the valence band (VB) of the semiconductor can be excited to its conduction band (CB) to generate electron (e^-) and hole (h^+) pairs. The photogenerated carriers then react with water or dissolved oxygen to produce reactive oxidizing species (ROS) such as hydroxyl radicals ($^\bullet OH$) and superoxide anions radicals ($^\bullet O_2^-$), and incorporate with the photogenerated holes to decompose pollutants into small molecules. However, although tens of thousands of papers have reported on the successful degradation of various pollutants [6–8], to the best of our knowledge, there is almost no study predicting whether these photocatalysts are able to degrade other kinds of contaminants or not. In other words, no research has answered the basic question of photocatalysis about what is the essential condition for the degradation of a particular contaminant. For instance, a photocatalyst has good catalytic activity for the photodegradation of typical pollutants such as rhodamine B (RhB) and methyl orange (MO) would imply it is

* Corresponding authors.
E-mail addresses: xiaox@scnu.edu.cn (X. Xiao), jmnan@scnu.edu.cn (J. Nan).

http://dx.doi.org/10.1016/j.apcatb.2016.05.042
0926-3373/

a good catalyst with extensive and practical application to other organic contaminants? Obviously, it is doubtful. This reveals the limited understanding of photocatalysis, which greatly weakens the research significance and environmental applications, and hinders an in-depth understanding of the photocatalytic mechanism as well.

In recent years, our group has worked continuously on bismuth-based photocatalysts for the visible-light photocatalytic degradation of pollutants with specific structures, especially phenolic pollutants [9–14]. And we have found: (1) The band structures of bismuth-based semiconductor, including bismuth oxyhalides and Bi-based double metal oxides, could be easily regulated by tailoring with bismuth, oxygen, type of halogen (or another metal), and their proportion. (2) Majority of narrow-band semiconductor materials, in particular bismuth-based semiconductors, are difficult to generate hydroxyl radicals through the reaction of the photogenerated holes with H_2O or OH^- under visible-light irradiation. Thus, the primarily oxide species are the photogenerated holes and superoxide radicals. Considering to the oxidizing power of $^{\bullet}O_2^-$ is not very strong, the oxidizing activity of these semiconductors will be determined by the oxidation ability of photogenerated holes. These findings inspire us to find out the relationships between the band structure of photocatalysts (especially for the valence band potential) and the molecular structure of pollutants (especially for the oxidation behaviors of organic contaminants), and subsequently to predict the essential conditions for the possibility of a photocatalytic degradation reaction.

To solve the above problems, herein, a series of photocatalytic experiments have been carried out using a variety of photocatalysts with different band structures to degrade varied pollutants. By combining the experimental results, basic theories of photocatalysis, and principles of physical chemistry (particular for the electrochemistry and computational chemistry), we summarize a new model called "semiconductor photo-induced electrocatalysis" (SPEC) to expatiate the reaction mechanism of the photocatalytic degradation and to better interpret what happens during photocatalytic process. More importantly, it is expected to predict the possibility of the reactions before the photodegradation experiments. From the viewpoint of photo-induced electrocatalysis, we can be more intuitive in the realization of different photocatalysis systems and easily predict, design, and develop effective photocatalysts for the degradation of a specific target contaminant.

2. Experimental

2.1. Materials

Bisphenol-A(BPA) and phenol were purchased from Sinopharm Group Chemical Reagent Co. Ltd. Methylparaben (MPB), propylparaben (PPB), and 4-hydroxy-2,2,6,6-tetramethylpiperidinyloxy (TEMPOL) were obtained from J&K Chemical Ltd. Bismuth nitrate pentahydrate ($Bi(NO_3)_3{\cdot}5H_2O$), potassium iodide (KI), potassium bromide (KBr), sodium oxalate, were purchased from Tianjin Kermel Chemical Reagent Co., Ltd. Ethylene glycol (EG) was bought from Chinasun Specialty Products Co., Ltd. Rhodamine B (RhB), tetracycline (TC), acetaminophen (APAP), isopropanol (IPA), and propionic acid (PA) were obtained from Aladdin Reagent Co., Ltd. All reagents were of analytical grade and used as-received without further purification.

2.2. Synthesis of the photocatalysts

The $Bi_4O_5I_2$ nanoflakes were synthesized using a solvothermal route according to the process described in our previous report [11]. Briefly, 1.5 mmol $Bi(NO_3)_3{\cdot}5H_2O$ and 3 mmol KI were dissolved in 35 mL EG, and the solution pH was adjusted to ~9 by a NaOH solution (2 mol L^{-1}). Afterwards, the mixture was transferred into a Teflon-lined stainless-steel autoclave and kept inside an electric oven at 140 °C for 12 h. After completion of the reaction, the precipitate was collected, washed with deionized water and ethanol, and finally dried at 60 °C. The BiOI nano-microspheres were produced using the same process but without adding the NaOH solution. The $Bi_4O_5Br_2$ nanoflakes were also synthesized using the same procedure, but KI was replaced by 1.5 mmol KBr.

2.3. Computational methods

The energies of the highest occupied molecular orbital (HOMO) and the lowest unoccupied molecular orbital (LUMO) of selected contaminants were calculated by density functional theory (DFT) using Gaussian 09. The optimized geometries and vibration frequencies were obtained using the B3LYP function, along with the 6-311++G(d,p) basis set. The band structure calculations of photocatalysts were conducted with the Cambridge Serial Total Energy Package (CASTEP) code within Materials Studio Package based on the density functional theory. The crystal data (ICSD #24610, #412590, and #94498 for BiOI, $Bi_4O_5I_2$, and $Bi_4O_5Br_2$, respectively, as shown in Fig. S1, Supporting information) were utilized as the original crystal models. The generalized gradient approximation (GGA) in the scheme of Perdew-Burke-Ernzerhof (PBE) was used for the exchange-correlation functional. Ultrasoft pseudopotentials were used for all chemical elements. The 2s and 2p states were considered for O with six electrons, ns and np (n = 4 and 5 for Br and I, respectively) states were used for Br or I with seven electrons, and 6s and 6p states were taken into account with five electrons of Bi. The kinetic energy cutoffs of 380 eV for the smooth part of the electronic wave functions to achieve a total-energy difference below 5.0×10^{-7} eV $atom^{-1}$, and 12 empty orbitals were implemented. The Brillouin zone was sampled with a Monkhorst-Pack k-point grid of $6 \times 6 \times 3$ to achieve a k-point separation about 0.04 $Å^{-1}$. The energies and electronic structures were calculated based on the optimized geometries.

2.4. Characterization

The crystalline structures of the samples were determined using powder X-ray diffraction (XRD) with a Bruker D8 Advance (Bruker AXS, Germany) X-ray diffractometer with Cu Kα radiation. The morphology was observed using a field-emission scanning electron microscope (FE-SEM, Zeiss Ultra 55, Germany). The specific surface areas were measured using nitrogen adsorption-desorption isotherms at 77 K according to the Brunauer-Emmett-Teller analysis (BET, Quadrasorb SI, Quantachrome Instruments, USA). A desorption isotherm was used to determine the pore size distribution using the Barrett-Joyner-Halenda (BJH) method. The UV–vis diffuse reflection spectra (DRS) were recorded on a UV–vis spectrophotometer (UV-3010, Hitachi, Japan) using $BaSO_4$ as a reference and were converted from reflection to absorbance by the Kubelka-Munk method. Electron paramagnetic resonance (EPR, JES FA-200, JEOL, Japan) in combination with spin-trapping techniques was utilized to detect free radicals, and 5,5-dimethyl-1-pyrroline-*N*-oxide (DMPO) was used as a spin trap.

Cyclic voltammetry (CV) was carried out on a CHI 910B (Shanghai Chenhua Apparatus Corporation, China) electrochemistry workstation with a scan rate of 50 mV s^{-1} in 0.1 mol L^{-1} HAc–NaAc buffer solution. A glassy carbon electrode (GCE), a platinum plate, and a saturated calomel electrode (SCE) were served as the working, counter, and reference electrodes, respectively. The redox potentials of target pollutants, including BPA and phenol, with different concentrations were evaluated from the results of voltammogram analyses. The CV measurement of

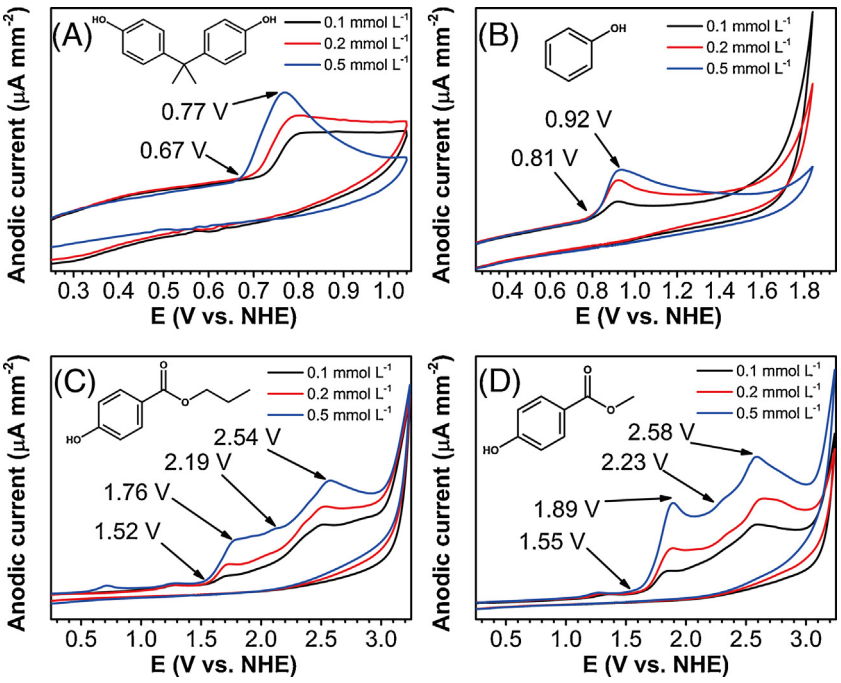

Fig. 1. The cyclic voltammograms of bisphenol A (A), phenol (B), propylparaben (C), and methylparaben (D) at different concentrations.

MPB and PPB were used the same method, but the electrolyte was altered by 0.1 mol L^{-1} $LiClO_4$ in CH_3CN. The Mott–Schottky experiments were conducted to evaluate the band positions of the as-synthesized samples with an electrochemistry workstation (Autolab PGSTAT302, Netherlands) using the photocatalyst as the working electrode (an appropriate amount of the sample suspension was deposited on conductive indium tin oxide glass), a platinum plate as the counter electrode, and a SCE as the reference electrode. A Na_2SO_4 aqueous solution (0.5 mol L^{-1}) was used as the electrolyte. The potential range was from −0.6 to 0.8 V at a constant frequency of 1000 Hz with steps of 10 mV. The flat band potentials of the samples were estimated from an intersection of a tangent with the x-axis. Then, the bottom of the conduction band was calculated as its flat band potential −0.1 V.

2.5. Degradation experiments

The photocatalytic activities of the photocatalysts were performed for the photocatalytic degradation of the target pollutants in aqueous solutions in a XPA-VII type photochemical reactor (Nanjing Xujiang Machine-electronic Plant, China), which was equipped with a 1000 W xenon lamp and a 420 nm cut-off filter. For a typical experiment, 50 mg of the as-prepared catalyst was dispersed in 50 mL contaminant solution (20 mg L^{-1} BPA, 10 mg L^{-1} phenol, PPB, or MPB). Prior to the irradiation, the mixture was stirred magnetically in the dark for 90 min to reach an adsorption-desorption equilibrium. During the photoreaction process, approximately 3 mL of the suspension was collected at specified times. Next, the solid was separated from the mixture using a 0.45 μm nitrocellulose filter, and the filtrate was then scanned by a UV–vis spectrophotometer (UV-1800, Shimadzu, Japan) between 190–800 nm.

3. Results and discussion

3.1. The molecular orbital energies and electrochemical behaviors of four contaminants

Four organic contaminants, including phenol, BPA, MPB, and PPB, were chosen for the investigation. The first two are typical phenolic compounds with estrogenic activity, the latter two are widely used preservatives and have revealed acute/chronic toxicity [15]. Consistent with above ideas, to clearly understand the necessary conditions for the effective photocatalytic degradation, the redox potentials of these pollutants are estimated prior to their degradation. According to molecular orbital theory [16,17], the tendency of a compound receiving or losing an electron is mainly dependent on the energy of highest occupied molecular orbital (HOMO) or the energy of lowest unoccupied molecular orbital (LUMO), respectively. In general, a higher HOMO energy means that the compound is easily oxidized, while a lower LUMO level implies that it is easily reduced, and the energy difference between the LUMO and HOMO can be used to estimate the stability of the compound. Then the occupied/unoccupied energies for above four compounds were calculated, and the results are shown in Table 1. It can clearly be seen that the HOMO energies of BPA, phenol, PPB, and MPB are gradually decreasing, which indicates that they are becoming more difficult to be oxidized (losing an electron).

Table 1
Molecular orbital energy calculations of four organic contaminants.

Contaminant	E_{HOMO}/eV	E_{LUMO}/eV	$\Delta E_{L\text{-}H}$/eV
BPA	−5.594	−0.056	5.539
Phenol	−5.958	0.036	5.993
PPB	−6.304	−0.915	5.389
MPB	−6.406	−0.953	5.453

The CV measurements were carried out to verify the prediction based on the calculations and to experimentally determine the oxidation potentials of these four compounds. As shown in Fig. 1, it is clearly shown that all of these chemicals can be oxidized at different potentials. For example, the oxidation reaction of BPA begins at 0.67 V (onset potential) versus normal hydrogen electrode (NHE), then a peak potential appears at of 0.77 V vs. NHE. These results suggest that if we would like to oxidize BPA, the oxidation potential must exceed 0.67 V, and the potential for the effective degradation requirement 0.77 V. The oxidation reactions for other three pollutants can also be similarly understood and predicted according to their CV profiles. In addition, there are two peaks in the potential range of PPB and MPB, which can be ascribed to their oxidation of

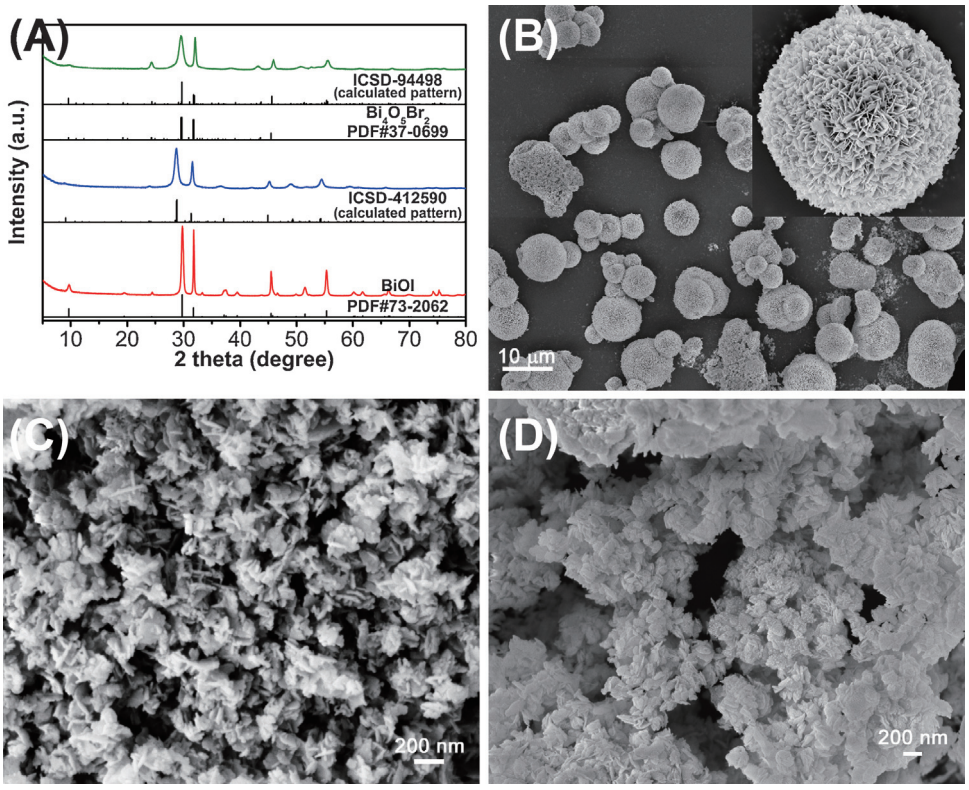

Fig. 2. (A) XRD patterns of the as-synthesized BiOI, $Bi_4O_5I_2$ and, $Bi_4O_5Br_2$; (B–D) SEM images of the as-synthesized BiOI (B), $Bi_4O_5I_2$ (C) and $Bi_4O_5Br_2$ (D).

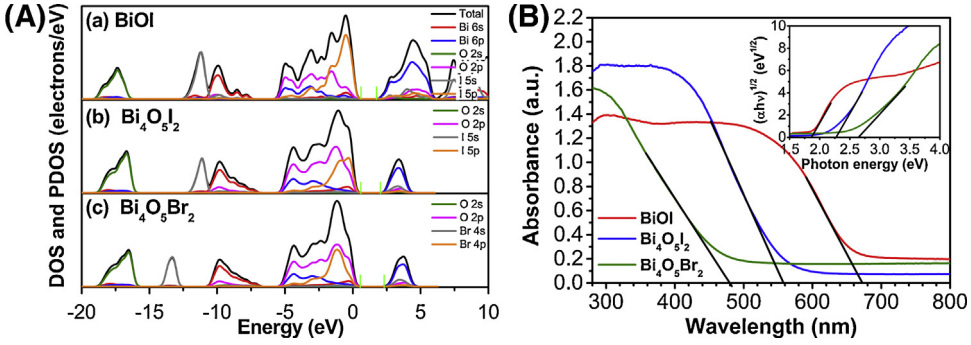

Fig. 3. (A) The density of states (DOS) and partial density of states (PDOS) for (a) BiOI, (b) $Bi_4O_5I_2$, and (c) $Bi_4O_5Br_2$; (B) UV–vis diffuse reflection spectra (DRS) of as-synthesized bismuth oxyhalides, the inset shows the plots of $(\alpha h\nu)^{1/2}$ vs. photon energy ($h\nu$).

hydroxyl group and carboxyl group [18], respectively. Obviously, the trend for the oxidation potentials of these compounds is in accordance with the results of quantum calculations.

In practice, it is often be confused on the interrelation between the units of eV (energy) and V (potential) in semiconductor photocatalysis. Considering there is only one electron transfer and about 4.5 eV energy is needed for the escape of an electron into the theoretical vacuum (0 eV), the following equation (Eq. (1)) can be used.

$$E(eV) = -4.5 - E(V) \times 1e \quad (1)$$

In fact, in the field of organic light-emitting semiconductors, for example, organic thin film transistor [19], organic photovoltaic device [20], and electroluminescence polymer [21], recent studies have confirmed that the frontier molecular orbital energy levels (HOMO/LUMO) of organic semiconductors can be directly calculated by CV technique. These results reveals that no difference exists, from the viewpoint of energy, on rising voltage to force a compound to lost an electron (ionization potential), or using light energy to do the same thing. According to Eq. (1), the oxidation potentials of BPA, phenol, PPB, and MPB are 1.094, 1.458, 1.804, and 1.906 V, respectively, which are close to but slightly larger than the experimental values. In particular, it can be observed that BPA has the lowest oxidation potential (Fig. 1), which means it is very easily destroyed by an oxidation process. This may be a key reason for that BPA has been eliminated by a variety of photocatalysts, as reported in the literatures [22–24]. Whereas, since the oxidation potentials of PPB and MPB are rather high, are there any so-called excellent photocatalysts that can effectively decompose these chemicals?

3.2. Structural characterization of three photocatalysts

Three typical bismuth oxyhalides (BiOXs), featured their good light absorption ability, unique crystal, and electronic structures [25], were chosen as the catalysts for the photodegradation reactions of phenol, BPA, MPB, and PPB. Based on the previous study [13], BiOXs with different compositions and band structures can easily be obtained by adjusting the O:X ratio and X type, which offers us an opportunity to explore the relationship between the

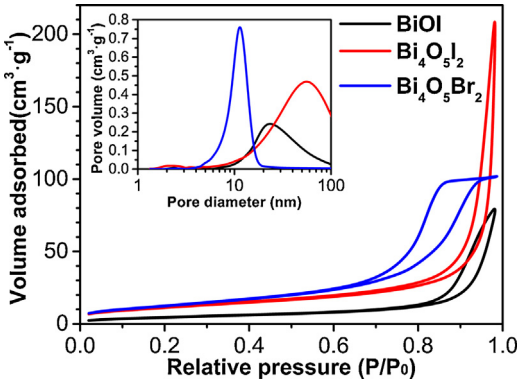

Fig. 4. Nitrogen adsorption-desorption isotherms and the corresponding pore size distribution curve (inset) for the as-synthesized BiOI, $Bi_4O_5I_2$, and $Bi_4O_5Br_2$.

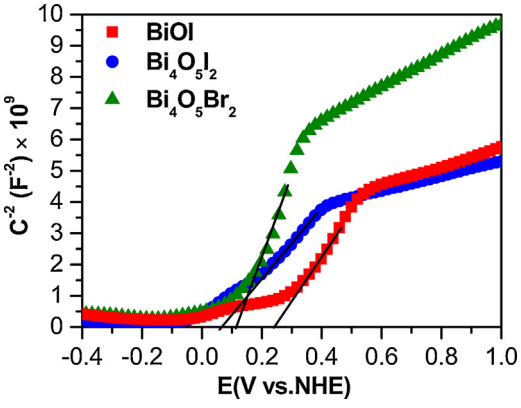

Fig. 5. Mott-Schottky plots for BiOI, $Bi_4O_5I_2$, and $Bi_4O_5Br_2$ electrodes.

photocatalytic activity and band structures of photocatalysts. By using a solvothermal route similar to our previous report [11], three bismuth oxyhalides were synthesized, and their XRD patterns are shown in Fig. 2A, which indicates their high degree of crystallinity and pure phases. The SEM images (Fig. 2B–D) further reveal that the synthetic materials are hierarchical microspheres (BiOI) and hierarchical nanoflakes ($Bi_4O_5I_2$ and $Bi_4O_5Br_2$).

The band structure and optical absorption feature of a semiconductor is considered as key factors to its photocatalytic performance [26]. To explore the impact of X type and O/X ratio on the electronic band structures of the as-synthesized materials, the density of states (DOS) for BiOI, $Bi_4O_5I_2$, and $Bi_4O_5Br_2$ were theoretically calculated according to their crystal structures (presented in Fig. S1, Supporting information) within density functional theory using the GGA-PBE functional. As shown in Fig. 3A, the valance band maximum (VBM) of BiOI mainly displays contribution from I 5p and O 2p states, while the Bi 6p and I 5s states dominate the conduction band minimum (CBM), resulting in a low bandgap energy. For $Bi_4O_5I_2$, i.e., increasing the content of oxygen whereas reducing the content of iodine, although the constituents of VBM and CBM are still combinations of I 5p/O 2p and Bi 6p/I 5s, respectively, the influence of O 2p on the VBM is increased, as has the contribution of I 5s to the CBM. When using bromine instead of iodine ($Bi_4O_5Br_2$), the roles of I 5p and I 5s in the VBM and CBM are replaced by Br 4p and Br 4s. Then the band-gap value of BiOI, $Bi_4O_5I_2$, and $Bi_4O_5Br_2$ were calculated to be 1.626, 2.362, and 2.453 eV, respectively, as shown in Fig. S2 (Supporting information). These results are ascribed to the fact that the electronegativity of nonmetallic atoms in these semiconductors follows the order I < Br < O, thus the band gaps of BiOI, $Bi_4O_5I_2$, and $Bi_4O_5Br_2$ are increasing gradually.

UV–vis diffuse reflectance spectroscopy (DRS) was conducted to evaluate the band gap energies (E_g) of as-synthesized bismuth oxyhalides. As shown in Fig. 3B, the maximal absorbance wavelengths of BiOI, $Bi_4O_5I_2$, and $Bi_4O_5Br_2$ are approximately 671, 557, and 479 nm, respectively, implying these photocatalysts can exhibit very good visible-light (λ > 420 nm) response. Their band gap energies were calculated using the following equation (Eq. (2)) [27]:

$$\alpha(h\nu) = A(h\nu - E_g)^{n/2} \quad (2)$$

where α, ν, E_g, and A are the absorption coefficient, light frequency, band gap energy, and a constant, respectively, and n is 4 for BiOXs' indirect transition [28]. Thus the E_g values of as-synthesized BiOI, $Bi_4O_5I_2$, and $Bi_4O_5Br_2$ were estimated from a plot of $(\alpha h\nu)^{1/2}$ as a function of the photon energy ($h\nu$) (inset of Fig. 3B) to be approximately 1.85, 2.26, and 2.56 eV, respectively.

It is worth noting that there are slight difference between theoretical calculations and experimental data, which can be ascribed to the fact that the current calculation method is imperfect. However, the advantages of DFT calculation are that it not only suggests the bandgap of a semiconductor but also presents more details about its energy band constituting, namely the contribution of each element and its orbital states in the composition on valence bands and conduction bands of the semiconductor. In addition, the composition and structure of a semiconductor can be modified using the software to gain altered models of materials and then theoretically calculated to predict their bandgaps and band structures, which will offers the possibility on the designing and developing unique photocatalysts.

The specific surface area of a photocatalyst is considered as another significant factor that affects its photocatalytic efficiency. As shown in Fig. 4, all of the isotherms of three samples correspond to type IV isotherm with a H3 hysteresis loop, suggesting their mesoporous features [29]. The BET surface areas were then calculated to be 17.02, 41.23, and 46.89 $m^2\,g^{-1}$ for BiOI microspheres, $Bi_4O_5I_2$ nanoflakes, and $Bi_4O_5Br_2$ nanoflakes, respectively. In addition, the corresponding pore size distributions of three photocatalysts were determined using the BJH method (inset in Fig. 4), which reveals that the average mesoporous diameters are 20.9, 57.1, and 11.2 nm for BiOI, $Bi_4O_5I_2$, and $Bi_4O_5Br_2$, respectively. The increasing of BET surface area of three photocatalysts are associated with their decreasing grain size (Fig. 2B–D), while the mesoporous structure most likely originate from their inter-nanoflake spacing [30].

3.3. Relationship between the band positions of catalysts and their catalytic feasibility

The energy band structures of as-synthesized samples were firstly evaluated using the following empirical equation (Eq. (3)) [31]:

$$E_{VB} = X - E^e + 0.5\,E_g \quad (3)$$

where E_{VB} is the valence band edge potentials, X is the electronegativity of the semiconductor, which is the geometric mean of the electronegativity of constituent atoms, E^e is the energy of free electrons on the hydrogen scale (about 4.5 eV), E_g is the band gap energy of the semiconductor, and E_{CB} (conductance band edge potentials) can be calculated by Eq. (4):

$$E_{CB} = E_{VB} - E_g \quad (4)$$

Consider the effect of pH value, the potentials of VB and CB for BiOXs at pH = 7 were calculated according to the next equation (Eq. (5)) [32]:

$$E = E^0 - 0.05915 \times pH \quad (5)$$

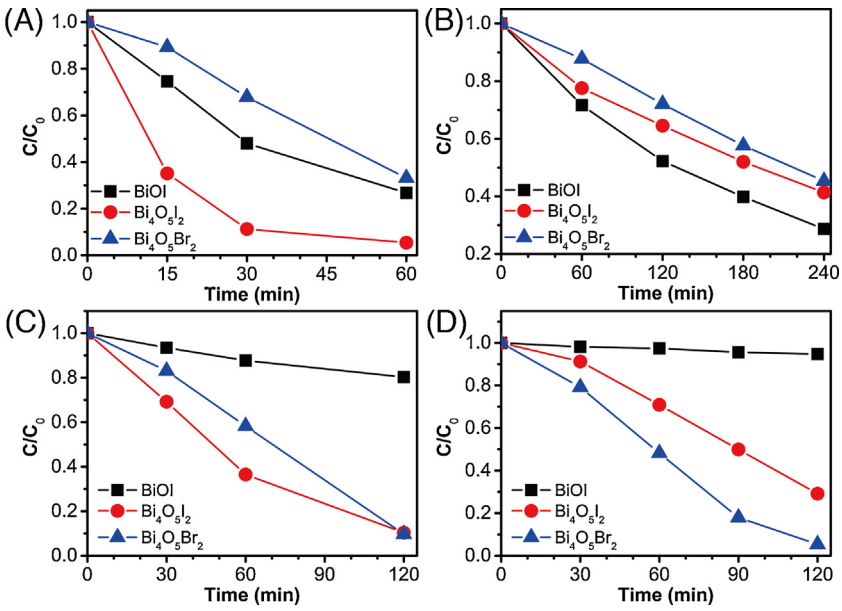

Fig. 6. Photocatalytic degradation of BPA (A), phenol (B), PPB (C), and MPB (D) over the as-synthesized BiOI, $Bi_4O_5I_2$, and $Bi_4O_5Br_2$ photocatalysts, respectively.

Table 2
Band positions of as-synthesized bismuth oxyhalides.

Photocatalyst	E_g/eV	Empirical		Experimental	
		E_{cb}/V	E_{vb}/V	E_{cb}/V	E_{vb}/V
BiOI	1.85	0.100	1.95	0.14	1.99
$Bi_4O_5I_2$	2.26	−0.115	2.15	−0.03	2.23
$Bi_4O_5Br_2$	2.56	−0.138	2.42	−0.01	2.55

Accordingly, the E_{VB} of as-prepared BiOI, $Bi_4O_5I_2$, and $Bi_4O_5Br_2$ are calculated to be 1.95, 2.15, and 2.42 V vs. NHE, while E_{CB} are estimated to be 0.100, −0.115, and −0.138 V vs. NHE, respectively, as presented in Table 2.

To experimentally estimate the exact band positions of as-synthesized bismuth oxyhalides, Mott–Schottky analysis were conducted [33]. As shown in Fig. 5, the flat band potential (V_{fb}) of the as-synthesized BiOI, $Bi_4O_5I_2$, and $Bi_4O_5Br_2$ electrodes are evaluated to be 0.24, −0.07, and −0.11 V vs. NHE, respectively. It is generally accepted that the CBM of a semiconductor is about 0.1 V more negative than its V_{fb}. Thus, the CBM of BiOI, $Bi_4O_5I_2$, and $Bi_4O_5Br_2$ are calculated to be 0.14, −0.03, and −0.01 V. Combined with the bandgap energy results assessed from the DRS analysis, the VB edge potentials of BiOI, $Bi_4O_5I_2$, and $Bi_4O_5Br_2$ are eventually given as 1.99, 2.23 and 2.55 V vs. NHE, respectively, which implies their oxidizing abilities are gradually increased. Then the experimental results are also showed in Table 2. Obviously, these results are consistent to the data predicted by empirical formula, which means that we can design a photocatalyst with desired band structure through adjusting different amount and type of atoms based on their electronegativities.

In order to evaluate the relationship between the photocatalytic activities with different structures of photocatalysts and contaminants, the photocatalytic performances of BiOI, $Bi_4O_5I_2$, and $Bi_4O_5Br_2$ against BPA, phenol, PPB, and MPB are shown in Fig. 6. Clearly, all of these photocatalysts can effectively degrade BPA and phenol because the oxidation potentials of these two phenolic compounds are rather low (Fig. 1A and B). Among them, $Bi_4O_5I_2$ presented the best activity for BPA decomposition, and BiOI showed the first position in removal of phenol. However, the $Bi_4O_5Br_2$ exhibited the worst performance in both cases, even though it has the highest specific surface area (Fig. 4) and the strongest oxidizing power (Table 2), showing the oxidizing power of photocatalysts is not a key role in these cases. Moreover, BiOI presented very poor photodegradation activity to PPB and MPB for they have higher oxidation potentials (Fig. 1C and D). This was especially true for MPB (takes the highest oxidation potential), where BIOI hardly exhibited activity (Fig. 6D), which may be ascribed to its lower VB position than the oxidation potential of MPB.

The results suggests that photocatalytic performance (dynamics related) is affected by various factors, and therefore a photocatalyst that shows higher activity for degrading one pollutant does not inevitably exhibit an advantage over other pollutants. And when the oxidation potential of a pollutant is low, the photodegradation result does not better even using a photocatalyst with a high oxidative ability. However, as the oxidation potentials of contaminants increased, $Bi_4O_5Br_2$, which possesses the highest valence band potential, clearly demonstrated its superiority. In fact, for the photocatalytic degradation of MPB, $Bi_4O_5Br_2$ not only displayed the best performance but also got a high mineralization efficiency (Fig. 7), whereas MPB was only partially oxidized by $Bi_4O_5I_2$ due to the latter's oxidation potential (~2.33 V) being lower than the second peak potential of MPB (2.58 V vs. NHE). The results suggest that when the degrading pollutants have higher oxidation potentials, the thermodynamic (energy) related factor may play a critical role, which may answer the question of photocatalysis that what is the essential condition for degradation of a particular contaminant.

The active species during the photocatalysis are very important to understand the photocatalytic reactions. To explore the oxygen species during the photodegradation on the three semiconductors, by using BPA as a model compound, free radicals trapping experiments were carried out. Among them, isopropanol, sodium oxalate, and TEMPOL were used to scavenge •OH, photogenerated h^+, and $•O_2^-$, respectively [34,35]. As shown in Fig. S3

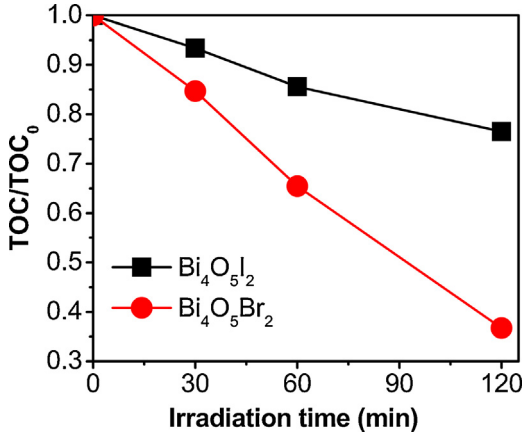

Fig. 7. TOC removal efficiencies of MPB over the as-synthesized $Bi_4O_5I_2$ and $Bi_4O_5Br_2$.

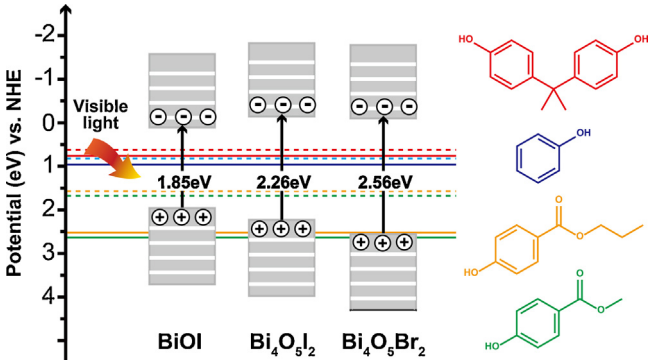

Scheme 1. Illustration of the band positions for the three photocatalysts and the oxidation potentials of four contaminants.

(Supporting information), these catalysts exhibit similar features that after the addition of isopropanol, the photocatalytic activities stay almost unchanged compared with no scavenger. Whereas an obvious inhibition can be observed in the existence of sodium oxalate and TEMPOL, which suggests that the photogenerated h^+ and $^{\bullet}O_2^-$ radicals, instead of by $^{\bullet}OH$ radicals, are playing key roles in these process. The results were further confirmed by EPR analysis (Fig. S4, Supporting information), which indications that obvious DMPO-$^{\bullet}O_2^-$ signals over the catalysts were detected after the visible-light irradiation.

In addition, there are other factors, such as the structure and surface area of catalysts, may greatly impact the photocatalytic activities. It can be observed from Fig. S2 that BiOI earns a good dispersion in its energy bands compared with other two photocatalysts, which may be benefit to its photocatalytic performance, especially for the elimination of containments with relatively lower oxidative potential. And although there is no regularity among the activities of different kinds of photocatalysts with their specific surface area in current cases, the same type of semiconductor having different structure and surface areas may exhibit different photocatalytic performances for degradation of identical pollutant. To verify this, another $Bi_4O_5Br_2$ sample was synthesized via room temperature hydrolysis route according to the literature [36]. This sample exhibited a different crystallinity and crystal face ratio (Fig. S5, Supporting information), specific surface area (Fig. S6, Supporting information), and photocatalytic activity for the degradation of MPB (Fig. S7, Supporting information) compared with the sample prepared by solvothermal method, displaying that the photocatalytic activity of a catalyst could be greatly affected by its structure and surface area.

3.4. Establishment of the semiconductor photo-induced electrocatalysis model

Considering the visible-light-driven photocatalytic process mainly dependent on direct holes oxidation instead of the indirect oxalated by hydroxyl radicals, the VB potential of a photocatalyst is an important factor to govern its oxidation capability. By comparing the band positions of the photocatalysts with the oxidation potentials of pollutants, the catalytic feasibility of three photocatalysts against four organic contaminants may well be explained. As shown in Scheme 1, different colors are used to distinguish between oxidation potentials of the four pollutants, and dotted lines represent their basic oxidation potentials (onset potential), whereas solid lines represent their optimal oxidation potentials (peak potential). When the VB potential of a photocatalyst is higher than the onset oxidation potentials of contaminants, the photodegradation process may occur, which can be understood as the organic is losing an electron and be oxidized by photogenerated holes on catalysts' surface. And if the valence band potential of a photocatalyst is positive than contaminant's peak oxidation potential, the significantly degradation maybe raised. Although BiOI has a high VB potential (approximately 2.0 V), when using O or Br partial replace of I, the VB edge potentials of $Bi_4O_5I_2$ and $Bi_4O_5Br_2$ can be further enhanced with their visible-light response properties remain, which will lead to higher oxidation ability.

It can be clearly seen from Scheme 1 that since the lower oxidation potentials of phenolic pollutants (phenol and BPA), the compounds can be easily degraded by available three photocatalysts. However, when come upon phenolic acid esters (MPB and PPB) which hold higher oxidation potentials, only photocatalysts with enough oxidation ability can photodegrade them. In other words, the more positive VB potential of a photocatalyst has thermodynamic advantage for oxidation degradation of a pollutant. Moreover, it is well known that a chemical reaction thermodynamically feasible does not means that it can react quickly. In fact, the photocatalytic reaction kinetics are affected by various factors such as structure, morphology, specific surface area, absorption property, photo-generated charge separation efficiency, interactions between catalysts and pollutants, and so on. This may explain the fact that although $Bi_4O_5Br_2$ has the strongest oxidation ability among three synthetic photocatalysts, it does not exhibit the best photocatalytic activity for all the cases, especially in degrading pollutants with lower oxidation potentials.

According to above results and analysis, a model for the reaction mechanism of photocatalytic degradation under visible-light irradiation from a viewpoint of photo-induced electrocatalysis (SPEC) is proposed. As shown in Scheme 2, the SPEC model can be divided into three perspectives. One is the "micro photochemical cell", namely, a short-circuited photoelectrochemical cell (PEC) [37], in which light energy is converted to electrical energy. However, if the photo-generated carriers are not able to be used rapidly, the majority of them will recombine and release their energy in the form of heat, which returns a low photoelectric conversion efficiency for the photocatalyst. Another part is the "micro electrolytic cell," wherein photo-generated electrons and holes on the photocatalyst surface show negative and positive potentials, respectively, like the cathode and anode of an electrolytic cell. By using the surfaces of particles as the electrode interface, substances in the system, such as organic pollutants, dissolved oxygen, water, H^+, and OH^-, are migrating to the electrodes surface and acting as electron acceptors (A) or electron donors (D). If the electrode potential is more positive (or more negative) than the oxidation (or reduction) potential, plus an overpotential, of reactants, the redox reactions will occur (electrolysis), whereby electrical energy is converted

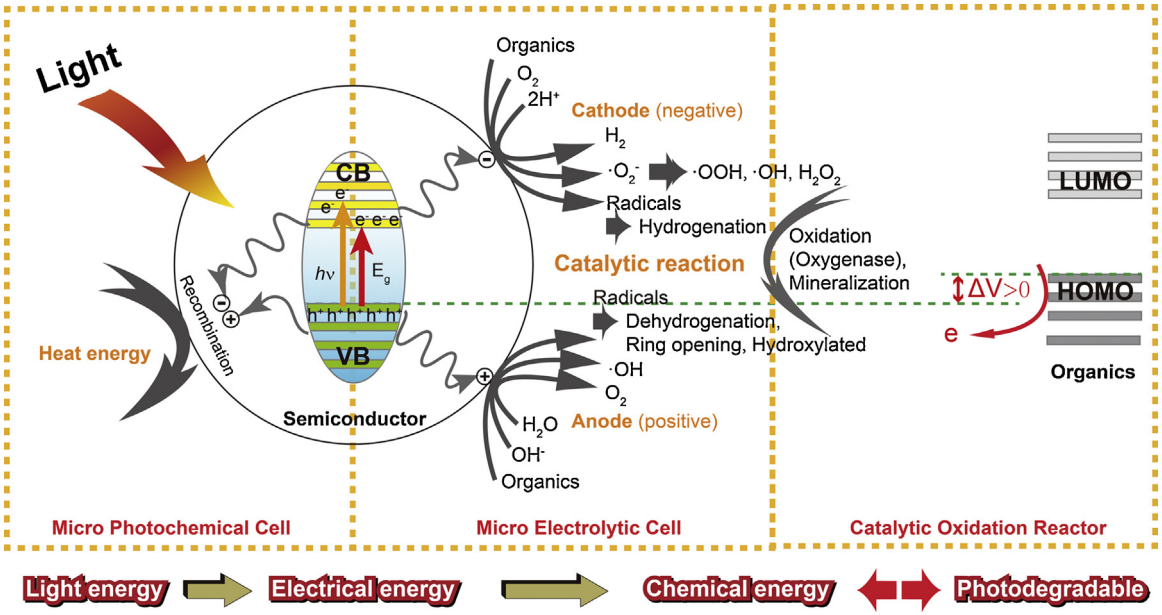

Scheme 2. The model of semiconductor photo-induced electrocatalysis.

Table 3
The theoretical and experimental prediction of pollutants degraded by synthetic catalysts.

Contaminant	Theoretical E_{HOMO}/eV	Ionization potential/V	Experimental potential		Degradation efficiency/%		
			onset/V	peak/V	BiOI	$Bi_4O_5I_2$	$Bi_4O_5Br_2$
Rhodamine B	−4.928	0.43	0.31	0.56	93.9	84.1	93.8
Tetracycline	−4.971	0.47	0.44	0.76	89.6	52.4	53.1
Acetaminophen	−5.848	1.35	0.64	0.85	90.5	62.2	44.8
Isopropanol	−7.094	2.59	1.83	2.18	53.7	57.3	69.9
Propionic acid	−7.478	2.98	2.23	2.74	0	0	0

to chemical energy. Like the traditional electrolytic cell, there are competitive reactions among these reactants on the micro-anode or micro-cathode, which is determined by the oxidation-reduction potential of reactants and the power of the photo-generated electrodes. The third part is the "catalytic oxidation reactor". When certain substances react with these photo-generated electrons or holes to produce radicals [38], such as $^{\bullet}O_2^-$, $^{\bullet}$OOH, $^{\bullet}$OH, and organic intermediates/radicals, catalytic reactions may take place (electrocatalysis). In this part, the frontier molecular orbital energy of organics is very important for it determines the first step of the reaction (lose or get an electron) can occur or not. Because the limitation of $^{\bullet}$OH radicals in the visible-light photocatalysis, the photo-generated holes is the main strong oxidants in these system, thus the initiation step of oxidation reaction will occur within the organics and photocatalysts when the VB potential of the semiconductor is positive than the oxidation potential of the organics ($\Delta V > 0$). And the oxidation potential of organics can be also predicted by their HOMO energy levels using Eq. (1) to convert potential and energy (i.e., a difference of 4.5 eV).

To prove the SPEC model is suitable for other contaminants, additional five different kinds of pollutants, which takes a totally different structures and properties, including rhodamine B (dye), tetracycline (antibiotic), acetaminophen (pharmaceutical), isopropanol (simple molecule), and propionic acid (carboxylic acid) were also selected as model contaminants to verify whether they can be degraded by as-synthesized catalysts. Before the photodegradation, the oxidation potential of contaminants were theoretical calculations and electrochemical measurements, and their ionization potentials were calculated by Eq. (1), then their photocatalytic degradation over as-synthesized three photocatalysts were evaluated under visible-light irradiation for 120 min, as shown in Table 3. The results clearly confirm that the electrochemical oxidation potentials of these pollutants match well with their theoretical predictions (ionization potentials), and the oxidation potentials of pollutants less than the VB potential of the photocatalysts is the necessary condition for their degradation. In fact, the propionic acid cannot be removed by all of these catalysts is attributed to its extremely high oxidation potential.

It must be clarified that the as-proposed system also has some distinct differences from the conventional electrolytic system. First, no power needs to be provided, because the illuminated semiconductor itself is a micro solar cell. Second, the micro electrodes (suspended micro/nanoscale particles while stirring) can be in sufficient contact with the reactants to resolve some of the weaknesses inherent to the traditional electrolytic reaction system, including the strong dependence of mass transfer on the electric field, the reliance of charge transfer on support electrolytes, and the need to quickly separate redox products from the electrode surfaces to sustain subsequent reactions. Thus, a higher electrolytic or electrocatalytic efficiency can be obtained using these micro electrodes. The third and essential difference is that the potential between the electrodes is not regulated by external power but decided by the band structure of the semiconductor material and the incident light energy. In other words, semiconductors with different compositions and structures may supply different oxidation and reduction abilities. For instance, the photo-generated electrons produced from TiO_2 and electrons produced by WO_3 under irradiation are the same as specie but different in energy (trend to loss of

it). This view is key point for applications of photocatalysis, as it can suggest us how to make a photocatalytic reaction takes place (possibility) in advance how to make it proceed faster (efficiency) [39], which has generally been overlooked by previous photocatalytic studies.

Therefore, so-called photocatalysis can be seen as a special photo-induced electrocatalytic process, which implies that we can use the knowledge of electrochemistry to obtain an original understanding of the photocatalysis and allow for the prediction and design of photocatalytic reactions. By using the SPEC model, we can answer the fundamental question of photocatalysis and estimate the probability of a photocatalytic reaction, and then find out or designs an appropriate photocatalyst for a target pollutant. Besides, following this prediction, the next step may involve improving the kinetic factors of the chosen reaction, such as reducing the overvoltage, increasing specific surface area of catalyst, promoting separate efficiency of photogenerated carriers, and further strengthen interactions between catalysts and contaminants.

4. Conclusions

In summary, by developing experiments of a variety of photocatalysts for degradation of different kinds of pollutants, a model of semiconductor photo-induced electrocatalysis system was successfully proposed, which clarifies the photocatalytic degradation mechanism from the viewpoint of energy (potential). By using the SPEC model and helped with electrochemical measurements and quantum chemical calculations, it is possible for predicting and controlling a specific photocatalytic reaction, which is determined by the relationship between the band positions of photocatalyst and the oxidation potentials of pollutants. This model might open new avenues for designing photocatalytic systems that can effectively decompose target pollutants and contribute to other important applications.

Acknowledgements

This work was financially supported by the National Natural Science Foundation of China (No. 21477040), the Guangdong Province Natural Science Foundation (Nos. 2015A030313393, S2012040007074).

Appendix A. Supplementary data

Supplementary data associated with this article can be found, in the online version, at http://dx.doi.org/10.1016/j.apcatb.2016.05.042.

References

[1] Y. Ma, Y. Jia, Z. Jiao, M. Yang, Y. Qi, Y. Bi, Chem. Commun. 51 (2015) 6655–6658.
[2] Y. Sasaki, H. Nemoto, K. Saito, A. Kudo, J. Phys. Chem. C 113 (2009) 17536–17542.
[3] T.S. Teets, D.G. Nocera, Chem. Commun. 47 (2011) 9268–9274.
[4] M. Matsumura, Y. Saho, H. Tsubomura, J. Phys. Chem. 87 (1983) 3807–3808.
[5] M. Elvington, J. Brown, S.M. Arachchige, K.J. Brewer, J. Am. Chem. Soc. 129 (2007) 10644–10645.
[6] L. Ye, J. Liu, Z. Jiang, T. Peng, L. Zan, Appl. Catal. B: Environ. 142–143 (2013) 1–7.
[7] X. Jin, L. Ye, H. Wang, Y. Su, H. Xie, Z. Zhong, H. Zhang, Appl. Catal. B: Environ. 165 (2015) 668–675.
[8] Q. Liu, D. Ma, Y. Hu, Y. Zeng, S. Huang, ACS Appl. Mater. Interfaces 5 (2013) 11927–11934.
[9] R. Hu, X. Xiao, S. Tu, X. Zuo, J. Nan, Appl. Catal. B: Environ. 163 (2015) 510–519.
[10] G. He, C. Xing, X. Xiao, R. Hu, X. Zuo, J. Nan, Appl. Catal. B: Environ. 170–171 (2015) 1–9.
[11] X. Xiao, C. Xing, G. He, X. Zuo, J. Nan, L. Wang, Appl. Catal. B: Environ. 148–149 (2014) 154–163.
[12] X. Xiao, R. Hu, C. Liu, C. Xing, C. Qian, X. Zuo, J. Nan, L. Wang, Appl. Catal. B: Environ. 140–141 (2013) 433–443.
[13] X. Xiao, C. Liu, R. Hu, X. Zuo, J. Nan, L. Li, L. Wang, J. Mater. Chem. 22 (2012) 22840–22843.
[14] X. Xiao, W. Zhang, J. Mater. Chem. 20 (2010) 5866–5870.
[15] Y. Gao, Y. Ji, G. Li, T. An, Water Res. 91 (2016) 77–85.
[16] N. San, A. Hatipoğlu, G. Koçtürk, Z. Çınar, J. Photochem. Photobiol. A: Chem. 146 (2002) 189–197.
[17] K. Fukui, T. Yonezawa, H. Shingu, J. Chem. Phys. 20 (1952) 722–725.
[18] J.R. Steter, R.S. Rocha, D. Dionísio, M.R. Lanza, A.J. Motheo, Electrochim. Acta 117 (2014) 127–133.
[19] M.L. Tang, A.D. Reichardt, P. Wei, Z. Bao, J. Am. Chem. Soc. 131 (2009) 5264–5273.
[20] B.C. Popere, A.M. Della Pelle, A. Poe, G. Balaji, S. Thayumanavan, Chem. Sci. 3 (2012) 3093–3102.
[21] Q. Sun, H. Wang, C. Yang, Y. Li, J. Mater. Chem. 13 (2003) 800–806.
[22] D.P. Subagio, M. Srinivasan, M. Lim, T. Lim, Appl. Catal. B: Environ. 95 (2010) 414–422.
[23] X. Xiao, R. Hao, M. Liang, X. Zuo, J. Nan, L. Li, W. Zhang, J. Hazard. Mater. 233 (2012) 122–130.
[24] Y. Liu, L. Deng, Y. Chen, F. Wu, N. Deng, J. Hazard. Mater. 139 (2007) 399–402.
[25] J. Jiang, K. Zhao, X. Xiao, L. Zhang, J. Am. Chem. Soc. 134 (2012) 4473–4476.
[26] J. Tang, Z. Zou, J. Ye, Angew. Chem. Int. Ed. 43 (2004) 4463–4466.
[27] X. Zhang, Z.H. Ai, F.L. Jia, L.Z. Zhang, J. Phys. Chem. C 112 (2008) 747–753.
[28] F. Qin, G. Li, R. Wang, J. Wu, H. Sun, R. Chen, Chem. Eur. J. 18 (2012) 16491–16497.
[29] K. Sing, D.H. Everett, R. Haul, L. Moscou, R.A. Pierotti, J. Rouquerol, T. Siemieniewska, Pure Appl. Chem. 57 (1985) 603–619.
[30] J. Zhang, F. Shi, J. Lin, D. Chen, J. Gao, Z. Huang, X. Ding, C. Tang, Chem. Mater. 20 (2008) 2937–2941.
[31] Y. Xu, M.A.A. Schoonen, Am. Mineral. 85 (2000) 543–556.
[32] J. Cao, B. Xu, H. Lin, B. Luo, S. Chen, Dalton Trans. 41 (2012) 11482–11490.
[33] J. Cao, X. Li, H. Lin, B. Xu, B. Luo, S. Chen, Mater. Lett. 76 (2012) 181–183.
[34] W. Wang, T.W. Ng, W.K. Ho, J. Huang, S. Liang, T. An, G. Li, J.C. Yu, P.K. Wong, Appl. Catal. B: Environ. 129 (2013) 482–490.
[35] W. Wang, Y. Yu, T. An, G. Li, H.Y. Yip, J.C. Yu, P.K. Wong, Environ. Sci. Technol. 46 (2012) 4599–4606.
[36] X. Mao, F. Xie, M. Li, Mater. Lett. 166 (2016) 296–299.
[37] L. Li, P.A. Salvador, G.S. Rohrer, Nanoscale 6 (2014) 24–42.
[38] H. Tong, S. Ouyang, Y. Bi, N. Umezawa, M. Oshikiri, J. Ye, Adv. Mater. 24 (2012) 229–251.
[39] U.I. Gaya, A.H. Abdullah, J. Photochem. Photobiol. C 9 (2008) 1–12.